A systematic view on influenza induced host shutoff

A systematic view on Influenza induced host shut-off

Adi Bercovich-Kinori[1*], Julie Tai[1*], Idit Anna Gelbart[1], Alina Shitrit[1], Shani Ben-Moshe[2], Yaron Drori[3,4], Shalev Itzkovitz[2], Michal Mandelboim[3,4] and Noam Stern-Ginossar[1#]

[1] Department of Molecular Genetics, Weizmann Institute of Science, Rehovot, Israel.

[2] Department of Molecular Cell Biology, Weizmann Institute of Science, Rehovot, Israel.

[3] Central Virology Laboratory, Ministry of Health, Chaim Sheba Medical Center, Ramat-Gan, Israel

[4] Department of Epidemiology and Preventive Medicine, School of Public Health, Sackler Faculty of Medicine, Tel-Aviv University, Tel-Aviv, Israel

[#] To whom correspondence should be addressed; noam.stern-ginossar@weizmann.ac.il

[*] Authors contributed equally to this work

Abstract

Host shutoff is a common strategy used by viruses to repress cellular mRNA translation and concomitantly allow the efficient translation of viral mRNAs. Here we use RNA-sequencing and ribosome profiling to explore the mechanisms that are being utilized by Influenza A virus (IAV) to induce host shutoff. We show that viral transcripts are not preferentially translated and instead the decline in cellular protein synthesis is mediated by viral takeover on the mRNA pool. Our measurements also uncover strong variability in the levels of cellular transcripts reduction, revealing that short transcripts are less affected by IAV. Interestingly, these mRNAs that are refractory to IAV infection are enriched in cell maintenance processes such as oxidative phosphorylation. Furthermore we show that the continuous oxidative phosphorylation activity is important for viral propagation. Our results advance our understanding of IAV-induced shutoff, and suggest a mechanism that facilitates the translation of genes with important housekeeping functions.

Introduction

Influenza A viruses (IAV) are included among the Orthomyxoviridae family of negative single-stranded, segmented RNA viruses. These viruses cause an infectious disease that constitutes an important public health problem and remains today an important cause of morbidity and mortality (1). Like all viruses, IAV is absolutely dependent on the host-cell protein synthesis machinery to produce its proteins. To ensure priority access to host translation machinery, many viruses utilize host shut-off mechanisms that eliminate competition from cellular transcripts (2). Host shut-off could be achieved by two complementary mechanisms: 1. Direct co-opting of the translation machinery by mechanisms that force better translation of viral mRNAs compared to their host counterparts. A classic example for this strategy is employed by poliovirus. It cleaves an essential host cap- binding protein, eIF4G, therefore preventing cap-dependent translation of host mRNAs while viral RNA translation stays unperturbed through the use of an internal ribosome entry site (3). 2. Viral-induced degradation of host mRNAs. This strategy is employed by several herpesviruses that express endonucleases which cleave host mRNAs, thereby eliminating the competition with host mRNA for the translation apparatus and ensuring efficient cap-dependent translation of viral mRNAs (4).

IAV has long been known to significantly shut-off host genes expression. Interestingly, it is one of the few viruses for which both direct translation co-opting and host mRNA degradation were suggested to play a prominent role in host shut-off (5,6). Although IAV mRNAs share the basic features with host mRNAs like a 5’ 7-methyl guanosine (m7G) cap and a 3’ poly-adenylate (poly(A)) tail, previous research suggested that influenza mRNAs are preferably translated due to features found in the 5’UTR of viral mRNAs (7–9). In addition host mRNA degradation has long been acknowledged (10). The 5’ m7G caps on viral transcripts are acquired by “cap-snatching”(11), this snatching allows the priming of viral mRNA synthesis but also leads to nascent host transcripts degradation. In addition, inhibition of polyadenylation of host pre-mRNA by IAV Nonstructural protein 1 (NS1) protein (12), and degradation of the host RNA

polymerase II complex (13) could contribute to the reduction in host transcripts in infected cells. Recently, a highly conserved IAV protein PA-X, possessing the PA endonuclease domain, was shown to selectively degrade host mRNAs (6), strongly suggesting that PA-X is a general influenza host shut-off endonuclease.

Although the discovery of PA-X has prompted new examination of the mechanisms that drive host shut-off during IAV infection (14–17), several fundamental questions remain unanswered: (a) To what extent does IAV change host mRNAs expression and translation?, (b) what is the relative contribution of host mRNA degradation versus direct manipulation of translation to host shut-off? (c) to what extent does the virus possess mechanisms to ensure more effective translation of its own mRNAs?

Here, we took a systemic approach to explore the relative contribution of direct co-opting of the translation machinery, and reduction of host RNA levels to the reduction in host proteins synthesis. To this end, we have used RNA sequencing (RNA-seq) and ribosome profiling (deep sequencing of ribosomes-protected fragments) to globally map the changes in host genes RNA and translation levels during IAV infection. These comprehensive and simultaneous measurements complemented with Single molecule Fluorescence in-situ Hybridization (smFISH) revealed that host shut-off is mainly achieved by reduction in cellular mRNAs levels, and that IAV transcripts are not preferably translated. Our systematic analysis also reveals that host transcripts are affected differently by IAV infection and that the extent of mRNAs reduction is related to their length and GC content. Interestingly, we noticed that transcripts encoding to oxidative phosphorylation related proteins are less affected by IAV infection, their proteins levels remain stable throughout infection and their continuous expression supports the energetic demands that are essential for virus replication.

Results:

Simultaneous monitoring of RNA levels and translation during IAV infection

To gain a detailed view of the changes that occur in viral and host transcripts abundance and translation over the course of IAV infection, we infected A549 cells with the A/Puerto Rico/8/1934 H1N1 (PR8) strain at MOI=5 and harvested cells at 2, 4, and 8 hours post infection (hpi). We designed our experiment to simultaneously monitor both RNA levels and translation (Fig. 1A). Deep sequencing of mRNA (RNA-seq) allows a detailed mapping of transcript levels during infection and these were paired with ribosome footprints, which allow accurate measurement of protein synthesis by capturing the overall *in vivo* distribution of ribosomes on a given message (18). In order to assess the reproducibility of our experiments we prepared two independent biological replicates for each of these time points. Both the mRNA and footprints read density measurements were reproducible (Fig. 1B). We quantitatively assessed the expression pattern of 7211 human transcripts and the 8 viral transcripts that are expressed from the 8 genomic segments of influenza. Metagene analysis, in which gene profiles are aligned and then averaged, revealed the expected profiles of footprints along mRNAs; ribosome density accumulates along the gene body ending at the first in-frame stop codon with pronounced accumulation of ribosomes at the initiation and termination sites (Fig. 2A). Unexpectedly, examination of the ribosome profiling data obtained from influenza transcripts revealed reads that align to the IAV minus strand (vRNA) that is non-coding (Fig 2B). These reads were not correlated with any sequence feature related to translation and were specific for the virus as individual human transcripts presented the expected profiles precluding any general problem in the sample preparation (Fig 2C). To test if the footprints we obtained from viral mRNAs indeed originate from ribosome protected fragments we generated an additional set of ribosome profiling libraries in which cells were pre-treated with harringtonine, a drug which leads to a strong accumulation of ribosomes precisely at translation initiation sites (18). As expected harringtonine treatment led to strong accumulation of ribosome

protected fragments at the first AUG and to depletion of ribosome density from the body of the viral and host mRNAs. Thus, this indicates that the protected fragments we captured from both cellular and viral mRNAs originate from ribosome protected fragments of transcripts that were engaged in active translation elongation (Fig 2A, 2B and 2D). In contrast, the protected fragments that mapped to the IAV minus strand were not affected by harringtonine treatment (Fig 2B and Figure 2- figure supplement 1) indicating that the protection of these fragments is probably not mediated by translating ribosomes.

To further illustrate that the footprints we obtained from viral mRNA reflect ribosome-protected fragments we applied a recently developed metric that distinguishes between 80S footprints and non-ribosomal sources using footprint size distributions (19). In ribosome-profiling data, the overall size distribution of fragments derived from protein-coding sequences, differs from the lengths of contaminating fragments found in profiling samples (19). We used a fragment length organization similarity score (FLOSS) that measures the magnitude of disagreement between the footprints distribution on a given transcript and the footprints distribution on canonical CDS. As expected thousands of well-expressed protein-coding transcripts scored well, and the similarity improved with increasing read counts ((19) and Fig. 2E). IAV mRNAs scored well in these matrixes and they did not differ from well-expressed human transcripts (Fig 2E, blue). However, reads from IAV minus strand could be clearly distinguished from annotated coding sequences (Fig 2E, red). We conclude that the protected fragments originating from minus strand viral RNA are not generated by ribosome protection. These fragments could originate from protection by the viral nucleoprotein (NP) that associates with viral genomes and was shown to sediment with viral RNAs (20). This possibility is supported by the observation that the numbers of protected reads originating from the IAV genome increases as the infection progresses (Figure 2- figure supplement 2).

IAV host shut-off is driven by reduced levels of host RNA but not reduced translation

In order to quantitatively evaluate if IAV evolved mechanisms to co-opt the cells' ribosomes we calculated the translation efficiency (TE) across our time course. TE is defined as the ratio of footprints to total mRNAs for a given gene and reflects how well a gene is being translated. We then compared the TE of human genes to that of viral genes at each of the time points along infection (Fig. 3A). The analysis shows that the viral genes translation efficiencies fall within the general range of host genes translation indicating that viral transcripts are not preferentially translated during IAV infection and that direct co-opting of the translation machinery does not play a dominant role in cellular gene shut-off. Instead, our systematic analysis demonstrates that host shut-off stems from viral dominance over the mRNA pool. At 8 hpi viral mRNAs take over 53.8% of the translation activity in the cells as 57.3% of the mRNAs in the cells are viral (Fig. 3B). These findings show that the relative reduction in cellular mRNA expression is the main cause for host shut-off during infection. Our analysis concurs with the finding that PA-X endonuclease activity plays a dominant role in host shut-off during IAV infection (6,14–17).

To confirm that our system indeed recapitulates the previous observations that IAV induces host shutoff (8,21), we monitored protein synthesis in IAV infected A549 cells by metabolic labeling. As was previously reported, also in our system IAV infection produced abundant quantities of virus polypeptides from 4 hpi and this was accompanied by reduced cellular protein synthesis (Figure 3- figure supplement 1).

Host transcripts are differently affected by IAV infection

Next we quantitatively assessed the expression pattern of cellular genes along IAV infection. Interestingly, 74% of host transcripts were reduced by more than 3-fold in their footprints densities along infection, reflecting the drastic shut-off in host protein synthesis (Table S1). We compared the expression of infected samples to mock sample and clustered the mRNA and footprints ratios using partitioning clustering. This approach allowed clustering of the cellular transcripts into 4 distinct classes based on similarities in temporal expression profiles in the RNA-seq and ribosome profiling data.

175 Overall we found that changes in ribosome footprints tracked the changes in transcripts
176 abundance (Fig. 3C), which is in line with host protein synthesis shut-off being driven by
177 the in reduction cellular RNA levels and not by direct interference with the translation
178 machinery. Interestingly although the majority of host transcripts were significantly
179 reduced during influenza infection, (cluster 1 and cluster 4, Fig. 3C) we identified
180 numerous genes that were significantly elevated (cluster 2, Fig. 3C) and genes that were
181 not significantly changed during influenza infection (cluster 3, Fig. 3C).
182 We next carried out GO term enrichment analysis for each of these four clusters.
183 As expected the small group of upregulated mRNAs was significantly enriched with
184 genes related to antiviral defense (cluster 2, Pval=6.9E-13), including Viperin and IDO1
185 that were previously shown to be elevated during IAV infection (22–24). Interestingly,
186 cluster 1 which is composed of mRNAs that are most drastically downregulated is
187 enriched with genes related to DNA repair and cell cycle (Pval=1.7E-17 and Pval=4.3E-
188 18 respectively) whereas cellular mRNAs that are barely affected by IAV infection
189 (cluster 3) are enriched with genes related to oxidative phosphorylation and for
190 transcripts encoding ribosomal proteins (Pval=3.4E-10 and Pval=3.9E-8, respectively).
191 These measurements and analysis reveal that the shut-off in host protein synthesis is
192 mainly driven by reduction in cellular mRNA levels and that host mRNAs sensitivity to
193 influenza is not uniform and certain mRNAs are more resistant to viral interference.
194 One limitation of global deep-sequencing measurements is that these
195 measurements provide relative but not absolute quantification of RNA and translation
196 levels. To address this issue we confirmed that there are no significant changes in the
197 overall levels of translation (Fig. 4B and (8)) and in total RNA (Table S2) along IAV
198 infection. We also extracted RNA from equal number of cells along infection and
199 performed real-time PCR analysis for cellular mRNAs from each of these clusters. These
200 independent measurements were in strong agreement with our RNA-seq measurements
201 (Fig. 3D).
202
203 ***Genes responsive to eIF2α phosphorylation are translationally induced after IAV***

infection

To quantitatively evaluate if there are genes that are differently translated along IAV infection, we used a computational framework named Babel (25). This analysis quantifies levels of ribosome occupancy higher or lower than those predicted from transcript abundance. In total, this approach allowed us to identify 210 cellular mRNAs that are differentially translated following IAV infection (Pval<0.01, Table S3). Among these, 125 genes were translationally upregulated whereas 85 genes were translationally down regulated. While Go enrichment analysis did not reveal any significant functional category, we noticed that within the group of translationally upregulated genes at 4 hpi, there was an enrichment for genes that were previously shown as translationally induced in conditions in which eukaryotic initiation factor 2α (eIF2α) is phosphorylated (pval<0.002, (26,27)). eIF2α phosphorylation is a stress response that reduces overall protein synthesis while enhancing translation of specific transcripts whose products support adaptive stress responses. By performing western blot analysis we show that at 4 hpi eIF2α phosphorylation is apparent and only at 8 hpi it is drastically reduced (Fig. 4A). By analyzing polysome profiles prepared from uninfected and IAV infected cells at 4 hpi, we confirmed that IAV infection indeed induce the translation of UCP2 and RALGDS (two genes that are also translationaly induced following stress induced eIF2α phosphorylation (26)), but not that of control genes SOX4 and SF3B5 for which no change in translation was observed (Fig. 4B and 4C and table S3). These results demonstrate that although IAV blocks eIF2α phosphorylation (28), at 4 hpi eIF2α phosphorylation affects cellular translation. In addition these findings provide another confirmation for the accuracy of our translation measurements.

smFISH measurements validate the RNA-seq quantification and reveal that cellular mRNA down regulation occurs in the nucleus

Our global measurements implied that host shut-off is driven by the high levels of IAV mRNAs that outnumber cellular transcripts, and that some cellular mRNAs are

less affected by IAV. We wanted to preclude normalization issues and to validate these observations using an independent quantification method that provides absolute measurements. To this end we used the smFISH technique that enables visualization of single mRNA molecules in fixed cells (29). This technique relies on the specific hybridization of short DNA libraries that are coupled to a fluorophore and are complementary to a specific target mRNA sequence. Binding of multiple probes to the same transcript yields a bright dot, indicative of a single mRNA molecule. This method has been used in various systems allowing accurate quantification of mRNA molecules per cell (30).

We quantified the expression of four human mRNAs, two mRNAs that are significantly reduced during influenza infection (*CHML* and *KIF18A*, cluster 1) and two mRNAs that were less affected by infection (*MYC* and *CDKN1B*, cluster 3). We also tested the expression of one viral transcript, *HA*. We designed a panel of fluorescently labeled probes, each composed of 48 20-base oligos complementary to the coding sequences of each of these genes. We used A549 cells that were left uninfected or IAV infected and then fixed at 2, 4, and 8 hpi. Hybridization of these cells with the fluorescently labeled probes libraries yielded bright diffraction-limited dots, representing single transcripts. These were automatically counted using a custom image-processing software (31). Importantly, when we examined *HA* expression in uninfected cells we did not detect any diffraction-limited dots demonstrating the specificity of this approach (Fig. 5A). Following infection with IAV, *HA* transcript levels were drastically elevated and at 8 hpi the intensity of the smFISH signal was too high to measure single dots (Fig. 5A). The expression levels of the four cellular transcripts we measured by smFISH were highly correlated with our RNA-seq measurements (Fig. 5A and 5B). These absolute quantifications of viral and host transcripts along IAV infection strongly support the notion that host shut-off is mainly driven by differences in mRNA levels. Furthermore, this data illustrates the variability in the levels of cellular transcripts reduction during IAV infection, suggesting that IAV-mediated degradation might act differently on different cellular transcripts.

Multiple mechanisms for IAV interference with cellular RNA expression have been described (7–11), all of which involve interference with processes occurring in the nucleus. The discovery of the highly conserved RNA endonuclease, PA-X, implied for the existence of cytoplasmic degradation machinery, since viral RNAses from other viruses were proposed to act in the cytoplasm (32). However, recent work presented evidence that PA-X activity might also be restricted to the nucleus (15). On top of absolute quantification, smFISH also provides spatial information about mRNA molecules distribution in the cell. This allowed us to test the levels of endogenous cellular transcripts in the nucleus and cytoplasm along influenza infection. We quantified the cytoplasmic and nuclear levels of *CHML* and *KIF8A*, which showed drastic reduction in their levels, and of *MYC* that showed subtler but still significant reduction (Fig. 5B). Interestingly, the nuclear and cytoplasmic levels of *CHML*, *KIF18A* and *MYC* were downregulated to the same extent (Fig. 5C). These results strongly suggest that interference in cellular RNA expression along IAV infection occurs mainly in the nucleus.

***Cellular transcripts reduction along IAV infection is correlated with transcripts' length and GC content*.**

We noticed that cellular genes respond differently to IAV infection and can be divided based on the level of reduction they present during infection (Fig. 3B, clusters 1, 3 and 4). Hence, we were interested in the features differentiating between these cellular mRNA groups. If IAV interference with cellular transcripts expression occurs mainly in the nucleus and there is no selectivity in this process then the decline in mRNA levels should be correlated with the cytoplasmic half-lives of mRNAs. Using recent measurements of mRNA half-lives in A549 cells (33) we identified a significant enrichment in mRNAs with long half-lives in cluster 3, which includes genes that were only mildly affected by IAV infection (Figure 5D, Pval=0.005), but this cluster contained also many genes with short half-life. These results suggest that there are additional features that govern the differences between these clusters, and that the differences in

290 the levels of reduction might stem from differences in IAV-interference with host genes
291 expression.
292 Since our measurements suggested that most of IAV mediated reduction occurs
293 in the nucleus and a recent study connected PA-X activity to the 3' end processing (15),
294 we tested whether the length of the poly-A tail affects the extent to which mRNAs are
295 reduced after IAV infection. Using genome wide measurements of poly-A tail length (34)
296 we did not observe any significant differences between the different clusters (Figure 5-
297 figure supplement 1). We next examined specific characteristics of the corresponding
298 transcripts, including their length and GC content. Interestingly, both mRNA length and
299 GC content showed a significant difference between the clusters and the transcripts that
300 were less affected by IAV were significantly shorter and had higher GC content (Fig. 5E
301 and 5F, Pval≤1.49e-63 and Pval≤3.636e-06, respectively). Since cluster 3 (composed of
302 genes that were less affected by IAV) is also significantly enriched in transcripts related
303 to oxidative phosphorylation and ribosomal proteins, and these functional categories
304 are composed of genes that tend to be short (Figure 5- figure supplement 2), we wanted
305 to exclude the possibility that the reduced length we observed is indirectly driven by the
306 enrichment in these functional categories. Indeed, also after omitting transcripts related
307 to these functional categories cluster 3 transcripts were significantly shorter (Figure 5-
308 figure supplement 2). Taken together these results strongly suggest that shorter and
309 more structured transcripts (transcripts with higher GC content) tend to be less effected
310 by IAV infection and therefore it is likely that the extent to which cellular mRNAs are
311 degraded is at least partially governed by the quantity of exposed single stranded RNA
312 in the nucleus.
313
314 ***The oxidative phosphorylation capacity is maintained late in IAV infection***
315 Host shut-off mechanisms clearly provide advantages for viruses as they hamper
316 the cellular response to infection and limit competition for cellular ribosomes. However,
317 dampening cellular gene expression also poses a big challenge, as viruses are fully
318 dependent on cellular resources such as macromolecules' building blocks, energy

319 production and the host translational machinery. Therefore, the observation that
320 transcripts coding for ribosomal and oxidative phosphorylation proteins, are less
321 reduced following IAV infection, implies that the translation maintenance of these
322 cellular pathways might be important for IAV infection. To validate this notion we
323 conducted western blot analysis on cell extracts along IAV infection and could confirm
324 the stable expression of components of the respiration complex (Fig.6A, upper panel),
325 whereas other proteins were reduced following IAV infection (Fig.6A, lower panel). In
326 accordance with these results, by staining infected cells with the potential sensitive
327 mitochondrial stain Tetramethylrhodamine (TMRM), we show that the mitochondria
328 membrane potential is not affected by IAV infection (Fig. 6B). Next we tested if
329 continuous oxidative phosphorylation is important for IAV propagation by employing
330 drugs that interfere with the function of respiratory chain. We used either the
331 ionophore Carbonyl cyanide m-chlorophenyl hydrazone (CCCP) or Valinomycin that
332 chelates potassium ions, both causing a collapses of the mitochondria membrane
333 potential. When cells were infected for 2 hours and then treated with CCCP or
334 Valinomycin in concentrations that did not affect cell viability (Figure 6- figure
335 supplement 1), IAV titers were significantly reduced (Fig. 6C and 6D). Overall, these
336 results indicate that mRNAs involved in oxidative phosphorylation are less perturbed by
337 IAV infection, and that maintenance of intact oxidative phosphorylation activity during
338 IAV infection is important for viral replication.
339

Discussion:

Many viruses have developed varied and sophisticated mechanisms to specifically repress cellular mRNA translation and concomitantly allow the selective translation of viral mRNA. In the case of IAV many mechanisms were suggested to contribute to the observed host shut-off. These include: 1. Cap-snatching of cellular pre-mRNAs (11), 2. Inhibition of cellular pre-mRNAs polyadenylation (12), 3. Degradation of RNA Polymerase I II (13), 4. Nuclear retention of cellular mRNAs (35), 5. Cellular mRNAs degradation (6,10,36) and 6. Preferential translation of viral mRNAs (5,7,8). Our systematic and unbiased analysis surprisingly demonstrates that viral mRNAs are not preferentially translated compared to their host counterparts and that the extensive translation of viral proteins is the result of viral takeover of the mRNA pool in the cell. These results are consistent with the notion that NS1 is not required for the shut-off of host cell protein production(37) and that PA-X endonuclease activity is a dominant factor in mediating host shut-off activity (6,14–17).

It should be noted that at 8 hpi there is already extensive viral replication (evident from the strong increase in reads originating from the viral minus strand). Therefore at this time point a portion of the viral RNA plus strand we measured are used as template for replication (cRNA) and not as mRNAs. Since our calculation of viral transcripts TE is based on dividing the number of footprints by the number of corresponding RNA reads it is possible that we underestimate the TE of viral genes at this time point. However, using our smFISH measurements for viral transcript we could show that >90% of the plus strand viral RNA is located in the cytoplasm. Therefore, this potential bias could result in maximum of 10% effect that does not hamper our conclusions.

Previous studies demonstrated inhibition of eIF2a phosphorylation during influenza infection and it was proposed that this inhibition is mediated by the activation of the cellular inhibitor of PKR, P58-IPK (28). Our analysis supports the observation that IAV infection inhibit eIF2a phosphorylation but we show that this inhibition is not immediate. In our experimental system eIF2a was phosphorylated at 4 hpi and this

stress response affects the expression of cellular genes (Figure 4). Since our measurements suggest the P58-IPK (DNAJC3) expression is reduced during IAV infection (by 3-fold) it is possible that other mechanisms also contribute to the inhibition of eIF2a phosphorylation.

Due to library normalization, it is challenging to assess from ribosome profiling and RNA-Seq measurements on overall virus-induced host shut-off. To address this inherent limitation we used smFISH, which allows absolute quantification of transcript levels in single cells. Our smFISH measurements correlated well with our global RNA quantification confirming our data and findings. In addition, our smFISH measurements show that after IAV infection RNA levels of endogenous cellular transcripts are reduced to a similar extent in the nucleus and the cytoplasm. This observation suggests that cellular mRNAs degradation occurs in the nucleus but it could also be explained by blockage of transcription in conjunction to cytoplasmic degradation that reduces cytoplasmic mRNA levels. The recent observation that PA-X activity is mostly nuclear (15) together with limited correlation with cytoplasmic half-life strongly points to the former possibility.

Our analysis also allowed us to quantify the reduction in cellular mRNAs along IAV infection, revealing that the extent of reduction varies between different transcripts. The magnitude of reduction could only be partially explained by cytoplasmic half-life and interestingly the extent of reduction was significantly correlated with transcript's length and GC content. Since cap-snatching activity was shown to target mostly small nuclear RNAs (38), it is likely that the majority of the observed differential reduction in cellular mRNAs is driven by PA-X degradation activity. Therefore, the relation to length and GC content strongly points to a non-selective process of degradation, where the chances of a transcript to be degraded are influenced by the quantity of exposed ssRNA. This notion is consistent with existing *In-vitro* data showing PA-X preference to ssRNA (17) and with the findings that PA-X lacks obvious sequence or location specificity (15). However, the notion that IAV induced degradation significantly depends on the length of the transcript does not easily reconcile with the evidence that

PA-X specifically targets Pol II transcripts and that this specificity is connected to 3' end processing (15). One way these results could be rationalized is if Pol II transcription and processing is physically limited to specific sub-nuclear compartments (39,40). In this case, the specificity of PA-X to Pol II transcripts could originate from physical proximity, while the recognition itself could be random and depends on the length and GC content, which will govern the amount of exposed ssRNA. Another possibility is that degradation activity is coupled to mRNA splicing. This can explain the specificity to Pol II transcripts and the relative resistance of short transcripts which intrinsically also tend to have less exons. However this possibility seems less favorable as at least by over expression PA-X did not affect the expression of cellular nascent transcripts (15). Future work focused on PA-X activity can help shed light on the exact mechanism.

Host shut-off is a common phenomenon, employed by diverse viruses and it is thought to contribute to viral progression in two main ways: by redirecting the translation machinery towards viral gene expression and by inhibiting cellular anti-viral responses. However, shutting off cellular protein production could also have adverse effects. Viruses are completely dependent on cellular resources and inhibiting cellular protein production can dampen processes that are indispensable for the virus. Interestingly, we noticed that transcripts that are less affected by IAV infection are enriched for genes involved in pathways that the virus potentially dependents on, such as oxidative phosphorylation components and ribosomal proteins. In contrast genes that were most significantly reduced are related to cell cycle, a cellular activity that is often blocked by viruses. Indeed, we were able to show that the levels of mitochondrial proteins are not affected by IAV even at 16 hpi, a time point in which other proteins were reduced. Further experiments demonstrated that inhibition of oxidative phosphorylation to levels that do not affect cell's viability severely impairs viral replication. These results suggest that continuous expression of proteins involved in oxidative phosphorylation is important for viral propagation. Since viruses mostly interfere with protein synthesis, the level of protein reduction during infection is also tightly connected to the half-life of these proteins. In this regard, the observation that

many of the proteins that perform basic cellular functions like translation and cellular respiration have long half-lives (41) could also assist viruses to avoid detrimental damage from shutting-off cellular protein synthesis. The inherent difficulties in blocking host protein production should be common to other viruses inducing host shut-off, particularly viruses with long infection cycle. It will therefore be interesting to see whether other viruses that interfere with cellular protein synthesis will also do this in a differential manner, facilitating the maintenance of cellular functions that are important for viral propagation.

It is well acknowledged that ribosome profiling is an emerging technique that allows probing of translation systematically and with increased sensitivity. This method in conjunction with RNA-seq was previously used to map the changes that occur in host gene expression during herpes simplex virus and cytomegalovirus infections (42,43) and to probe the complexity of several viruses (44–47). Here we show how these methods in conjunction with smFISH could be used to accurately quantify host shut-off along viral infection. These unbiased and systematic quantification methods can advance our understanding of viral interference with host protein production and are applicable to infection with any virus.

Acknowledgments

We thank Yossef Shaul, Nina Reuven, Ofer Mandelboim and NS-G lab members for critical reading of the manuscript. This research was supported by a research grant from Mr. Ilan Gluzman, The Human Frontiers Science Program Career Development Award, the EU-FP7-PEOPLE Career integration grant, the ICORE (Chromatin and RNA Gene Regulation), the Israeli Science Foundation (1073/14) and the European Research Council starting grant (StG-2014-638142). NS-G is incumbent of the skirball career development chair in new scientist.

References

1. Fields B. Fields virology. Philadelphia: Wolters Kluwer Health/Lippincott Williams & Wilkins; 2007.
2. Walsh D, Mathews MB, Mohr I. Tinkering with translation: protein synthesis in virus-infected cells. Cold Spring Harb Perspect Biol [Internet]. 2012/12/05 ed. 2013;5(1):a012351. Available from: http://www.ncbi.nlm.nih.gov/pubmed/23209131
3. Ventoso I, MacMillan SE, Hershey JW, Carrasco L. Poliovirus 2A proteinase cleaves directly the eIF-4G subunit of eIF-4F complex. FEBS Lett [Internet]. 1998 Sep 11 [cited 2016 May 4];435(1):79–83. Available from: http://www.ncbi.nlm.nih.gov/pubmed/9755863
4. Glaunsinger BA, Ganem DE. Messenger RNA turnover and its regulation in herpesviral infection. Adv Virus Res [Internet]. 2006/08/01 ed. 2006;66:337–94. Available from: http://www.ncbi.nlm.nih.gov/pubmed/16877064
5. Yanguez E, Nieto A. So similar, yet so different: selective translation of capped and polyadenylated viral mRNAs in the influenza virus infected cell. Virus Res [Internet]. 2011/01/05 ed. 2011;156(1-2):1–12. Available from: http://www.ncbi.nlm.nih.gov/pubmed/21195735
6. Jagger BW, Wise HM, Kash JC, Walters KA, Wills NM, Xiao YL, et al. An overlapping protein-coding region in influenza A virus segment 3 modulates the host response. Science (80-) [Internet]. 2012/06/30 ed. 2012;337(6091):199–204. Available from: http://www.ncbi.nlm.nih.gov/pubmed/22745253
7. Garfinkel MS, Katze MG. Translational control by influenza virus. Selective translation is mediated by sequences within the viral mRNA 5'-untranslated region. J Biol Chem [Internet]. 1993 Oct 25 [cited 2016 May 4];268(30):22223–6. Available from: http://www.ncbi.nlm.nih.gov/pubmed/8226725
8. Katze MG, DeCorato D, Krug RM. Cellular mRNA translation is blocked at both initiation and elongation after infection by influenza virus or adenovirus. J Virol [Internet]. 1986 Dec [cited 2016 May 4];60(3):1027–39. Available from: http://www.pubmedcentral.nih.gov/articlerender.fcgi?artid=253342&tool=pmcentrez&rendertype=abstract
9. Park YW, Katze MG. Translational control by influenza virus. Identification of cis-acting sequences and trans-acting factors which may regulate selective viral mRNA translation. J Biol Chem [Internet]. 1995 Nov 24 [cited 2016 May 4];270(47):28433–9. Available from: http://www.ncbi.nlm.nih.gov/pubmed/7499349
10. Beloso A, Martínez C, Valcárcel J, Santarén JF, Ortín J. Degradation of cellular mRNA during influenza virus infection: its possible role in protein synthesis shutoff. J Gen Virol [Internet]. 1992 Mar [cited 2015 Aug 5];73 (Pt 3):575–81. Available from: http://www.ncbi.nlm.nih.gov/pubmed/1545220
11. Plotch SJ, Bouloy M, Ulmanen I, Krug RM. A unique cap(m7GpppXm)-dependent influenza virion endonuclease cleaves capped RNAs to generate the primers that initiate viral RNA transcription. Cell. 1981 Mar;23(3):847–58.

12. Nemeroff ME, Barabino SM, Li Y, Keller W, Krug RM. Influenza virus NS1 protein interacts with the cellular 30 kDa subunit of CPSF and inhibits 3'end formation of cellular pre-mRNAs. Mol Cell [Internet]. 1998 Jun [cited 2016 Mar 28];1(7):991–1000. Available from: http://www.ncbi.nlm.nih.gov/pubmed/9651582
13. Rodriguez A, Pérez-González A, Nieto A. Influenza virus infection causes specific degradation of the largest subunit of cellular RNA polymerase II. J Virol [Internet]. 2007 May [cited 2016 May 16];81(10):5315–24. Available from: http://www.pubmedcentral.nih.gov/articlerender.fcgi?artid=1900203&tool=pmcentrez&rendertype=abstract
14. Khaperskyy DA, McCormick C. Timing Is Everything: Coordinated Control of Host Shutoff by Influenza A Virus NS1 and PA-X Proteins. J Virol [Internet]. 2015 Jul 1 [cited 2016 May 4];89(13):6528–31. Available from: http://jvi.asm.org/content/89/13/6528.long
15. Khaperskyy DA, Schmaling S, Larkins-Ford J, McCormick C, Gaglia MM. Selective Degradation of Host RNA Polymerase II Transcripts by Influenza A Virus PA-X Host Shutoff Protein. PLoS Pathog [Internet]. Public Library of Science; 2016 Feb 5 [cited 2016 May 4];12(2):e1005427. Available from: http://journals.plos.org/plospathogens/article?id=10.1371/journal.ppat.1005427#ppat.1005427.ref032
16. Khaperskyy DA, Emara MM, Johnston BP, Anderson P, Hatchette TF, McCormick C. Influenza a virus host shutoff disables antiviral stress-induced translation arrest. PLoS Pathog [Internet]. 2014 Jul [cited 2016 May 4];10(7):e1004217. Available from: http://www.pubmedcentral.nih.gov/articlerender.fcgi?artid=4092144&tool=pmcentrez&rendertype=abstract
17. Bavagnoli L, Cucuzza S, Campanini G, Rovida F, Paolucci S, Baldanti F, et al. The novel influenza A virus protein PA-X and its naturally deleted variant show different enzymatic properties in comparison to the viral endonuclease PA. Nucleic Acids Res [Internet]. 2015 Oct 30 [cited 2016 May 4];43(19):9405–17. Available from: http://www.pubmedcentral.nih.gov/articlerender.fcgi?artid=4627086&tool=pmcentrez&rendertype=abstract
18. Ingolia NT, Lareau LF, Weissman JS. Ribosome profiling of mouse embryonic stem cells reveals the complexity and dynamics of mammalian proteomes. Cell [Internet]. 2011/11/08 ed. 2011;147(4):789–802. Available from: http://www.ncbi.nlm.nih.gov/pubmed/22056041
19. Ingolia NT, Brar GA, Stern-Ginossar N, Harris MS, Talhouarne GJS, Jackson SE, et al. Ribosome Profiling Reveals Pervasive Translation Outside of Annotated Protein-Coding Genes. Cell Rep. 2014;8(5):1365–79.
20. Duesberg PH. Distinct subunits of the ribonucleoprotein of influenza virus. J Mol Biol [Internet]. 1969 Jun 28 [cited 2016 May 18];42(3):485–99. Available from: http://www.ncbi.nlm.nih.gov/pubmed/5804156
21. Skehel JJ. Polypeptide synthesis in influenza virus-infected cells. Virology [Internet]. Academic Press; 1972 Jul [cited 2016 Jul 31];49(1):23–36. Available

from: http://linkinghub.elsevier.com/retrieve/pii/S0042682272800047
22. Ranaware PB, Mishra A, Vijayakumar P, Gandhale PN, Kumar H, Kulkarni DD, et al. Genome Wide Host Gene Expression Analysis in Chicken Lungs Infected with Avian Influenza Viruses. PLoS One [Internet]. 2016 Jan [cited 2016 May 4];11(4):e0153671. Available from: http://www.pubmedcentral.nih.gov/articlerender.fcgi?artid=4829244&tool=pmcentrez&rendertype=abstract
23. Wang X, Hinson ER, Cresswell P. The interferon-inducible protein viperin inhibits influenza virus release by perturbing lipid rafts. Cell Host Microbe [Internet]. 2007 Aug 16 [cited 2016 May 4];2(2):96–105. Available from: http://www.ncbi.nlm.nih.gov/pubmed/18005724
24. Huang L, Li L, Klonowski KD, Tompkins SM, Tripp RA, Mellor AL. Induction and role of indoleamine 2,3 dioxygenase in mouse models of influenza a virus infection. PLoS One [Internet]. 2013 Jan [cited 2016 May 4];8(6):e66546. Available from: http://www.pubmedcentral.nih.gov/articlerender.fcgi?artid=3681773&tool=pmcentrez&rendertype=abstract
25. Olshen AB, Hsieh AC, Stumpf CR, Olshen RA, Ruggero D, Taylor BS. Assessing gene-level translational control from ribosome profiling. Bioinformatics [Internet]. 2013 Dec 1 [cited 2016 Mar 29];29(23):2995–3002. Available from: http://www.pubmedcentral.nih.gov/articlerender.fcgi?artid=3834798&tool=pmcentrez&rendertype=abstract
26. Andreev DE, O'Connor PB, Fahey C, Kenny EM, Terenin IM, Dmitriev SE, et al. Translation of 5' leaders is pervasive in genes resistant to eIF2 repression. Elife. 2015 Jan;4:e03971.
27. Sidrauski C, McGeachy AM, Ingolia NT, Walter P. The small molecule ISRIB reverses the effects of eIF2α phosphorylation on translation and stress granule assembly. Elife. 2015 Jan;4.
28. Goodman AG, Smith JA, Balachandran S, Perwitasari O, Proll SC, Thomas MJ, et al. The cellular protein P58IPK regulates influenza virus mRNA translation and replication through a PKR-mediated mechanism. J Virol [Internet]. 2007 Mar 1 [cited 2016 May 16];81(5):2221–30. Available from: http://jvi.asm.org/content/81/5/2221.abstract
29. Raj A, van den Bogaard P, Rifkin SA, van Oudenaarden A, Tyagi S. Imaging individual mRNA molecules using multiple singly labeled probes. Nat Methods [Internet]. Nature Publishing Group; 2008 Oct [cited 2016 Mar 25];5(10):877–9. Available from: http://dx.doi.org/10.1038/nmeth.1253
30. Itzkovitz S, van Oudenaarden A. Validating transcripts with probes and imaging technology. Nat Methods [Internet]. 2011/04/06 ed. 2011;8(4 Suppl):S12–9. Available from: http://www.ncbi.nlm.nih.gov/pubmed/21451512
31. Bahar Halpern K, Itzkovitz S. Single molecule approaches for quantifying transcription and degradation rates in intact mammalian tissues. Methods [Internet]. 2016 Apr 1 [cited 2016 May 16];98:134–42. Available from: http://www.ncbi.nlm.nih.gov/pubmed/26611432
32. Abernathy E, Glaunsinger B. Emerging roles for RNA degradation in viral

replication and antiviral defense. Virology [Internet]. 2015 May [cited 2016 May 20];479-480:600–8. Available from: http://www.sciencedirect.com/science/article/pii/S0042682215000501

33. Maekawa S, Imamachi N, Irie T, Tani H, Matsumoto K, Mizutani R, et al. Analysis of RNA decay factor mediated RNA stability contributions on RNA abundance. BMC Genomics [Internet]. 2015 Jan [cited 2016 May 20];16:154. Available from: http://www.pubmedcentral.nih.gov/articlerender.fcgi?artid=4359779&tool=pmcentrez&rendertype=abstract

34. Chang H, Lim J, Ha M, Kim VN. TAIL-seq: genome-wide determination of poly(A) tail length and 3' end modifications. Mol Cell [Internet]. 2014 Mar 20 [cited 2016 Apr 28];53(6):1044–52. Available from: http://www.ncbi.nlm.nih.gov/pubmed/24582499

35. Fortes P, Beloso A, Ortín J. Influenza virus NS1 protein inhibits pre-mRNA splicing and blocks mRNA nucleocytoplasmic transport. EMBO J [Internet]. 1994 Feb 1 [cited 2016 May 16];13(3):704–12. Available from: http://www.pubmedcentral.nih.gov/articlerender.fcgi?artid=394862&tool=pmcentrez&rendertype=abstract

36. Inglis SC. Inhibition of host protein synthesis and degradation of cellular mRNAs during infection by influenza and herpes simplex virus. Mol Cell Biol [Internet]. 1982 Dec [cited 2015 Aug 5];2(12):1644–8. Available from: http://www.pubmedcentral.nih.gov/articlerender.fcgi?artid=369973&tool=pmcentrez&rendertype=abstract

37. Salvatore M, Basler CF, Parisien J-P, Horvath CM, Bourmakina S, Zheng H, et al. Effects of influenza A virus NS1 protein on protein expression: the NS1 protein enhances translation and is not required for shutoff of host protein synthesis. J Virol [Internet]. 2002 Feb [cited 2016 May 16];76(3):1206–12. Available from: http://www.pubmedcentral.nih.gov/articlerender.fcgi?artid=135795&tool=pmcentrez&rendertype=abstract

38. Koppstein D, Ashour J, Bartel DP. Sequencing the cap-snatching repertoire of H1N1 influenza provides insight into the mechanism of viral transcription initiation. Nucleic Acids Res [Internet]. 2015 May 26 [cited 2016 May 11];43(10):5052–64. Available from: http://www.pubmedcentral.nih.gov/articlerender.fcgi?artid=4446424&tool=pmcentrez&rendertype=abstract

39. Mitchell JA, Fraser P. Transcription factories are nuclear subcompartments that remain in the absence of transcription. Genes Dev [Internet]. 2008 Jan 1 [cited 2016 May 16];22(1):20–5. Available from: http://genesdev.cshlp.org/content/22/1/20.abstract

40. Ghamari A, van de Corput MPC, Thongjuea S, van Cappellen WA, van Ijcken W, van Haren J, et al. In vivo live imaging of RNA polymerase II transcription factories in primary cells. Genes Dev [Internet]. 2013 Apr 1 [cited 2016 May 29];27(7):767–77. Available from: http://www.pubmedcentral.nih.gov/articlerender.fcgi?artid=3639417&tool=pmcentrez&rendertype=abstract

41. Schwanhausser B, Busse D, Li N, Dittmar G, Schuchhardt J, Wolf J, et al. Global quantification of mammalian gene expression control. Nature [Internet]. 2011/05/20 ed. 2011;473(7347):337–42. Available from: http://www.ncbi.nlm.nih.gov/pubmed/21593866
42. Rutkowski AJ, Erhard F, L'Hernault A, Bonfert T, Schilhabel M, Crump C, et al. Widespread disruption of host transcription termination in HSV-1 infection. Nat Commun [Internet]. 2015 Jan [cited 2016 Apr 5];6:7126. Available from: http://www.pubmedcentral.nih.gov/articlerender.fcgi?artid=4441252&tool=pmcentrez&rendertype=abstract
43. Tirosh O, Cohen Y, Shitrit A, Shani O, Le-Trilling VTK, Trilling M, et al. The Transcription and Translation Landscapes during Human Cytomegalovirus Infection Reveal Novel Host-Pathogen Interactions. PLoS Pathog [Internet]. 2015 Jan [cited 2016 May 16];11(11):e1005288. Available from: http://www.pubmedcentral.nih.gov/articlerender.fcgi?artid=4658056&tool=pmcentrez&rendertype=abstract
44. Stern-Ginossar N, Weisburd B, Michalski A, Le VT, Hein MY, Huang SX, et al. Decoding human cytomegalovirus. Science (80-) [Internet]. 2012/11/28 ed. 2012;338(6110):1088–93. Available from: http://www.ncbi.nlm.nih.gov/pubmed/23180859
45. Arias C, Weisburd B, Stern-Ginossar N, Mercier A, Madrid AS, Bellare P, et al. KSHV 2.0: A Comprehensive Annotation of the Kaposi's Sarcoma-Associated Herpesvirus Genome Using Next-Generation Sequencing Reveals Novel Genomic and Functional Features. PLoS Pathog. 2014;10(1).
46. Yang Z, Cao S, Martens CA, Porcella SF, Xie Z, Ma M, et al. Deciphering Poxvirus Gene Expression by RNA Sequencing and Ribosome Profiling. J Virol [Internet]. 2015 Apr 22 [cited 2015 Apr 27]; Available from: http://www.ncbi.nlm.nih.gov/pubmed/25903347
47. Irigoyen N, Firth AE, Jones JD, Chung BY-W, Siddell SG, Brierley I. High-Resolution Analysis of Coronavirus Gene Expression by RNA Sequencing and Ribosome Profiling. PLoS Pathog [Internet]. 2016 Feb [cited 2016 May 16];12(2):e1005473. Available from: http://www.pubmedcentral.nih.gov/articlerender.fcgi?artid=4769073&tool=pmcentrez&rendertype=abstract
48. Hindiyeh M, Levy V, Azar R, Varsano N, Regev L, Shalev Y, et al. Evaluation of a multiplex real-time reverse transcriptase PCR assay for detection and differentiation of influenza viruses A and B during the 2001-2002 influenza season in Israel. J Clin Microbiol [Internet]. 2005 Feb [cited 2016 May 25];43(2):589–95. Available from: http://www.pubmedcentral.nih.gov/articlerender.fcgi?artid=548105&tool=pmcentrez&rendertype=abstract
49. Huang DW, Sherman BT, Lempicki RA. Systematic and integrative analysis of large gene lists using DAVID bioinformatics resources. Nat Protoc [Internet]. 2009 Jan [cited 2014 Jul 9];4(1):44–57. Available from: http://www.ncbi.nlm.nih.gov/pubmed/19131956

675
676

Fig. 1

(A) Experiment set up of Ribosome profiling and RNA-seq along IAV infection. **(B)** Reproducibility of the ribosome footprints and mRNA measurements of host genes at 4 hpi. The correlation in footprints and mRNA measurements between biological replicates is presented.

Fig. 2

(A) Metagene analysis of ribosome profiling data. Average ribosome read density profiles over well-expressed genes, aligned at their start codon and stop codons. Data from uninfected, 2, 4 and 8 hpi samples, and harringtonine pretreated 8 hpi sample. **(B)** Ribosome occupancies following treatments (illustrated on the left) with cycloheximide (CHX, top panels), and harringtonine (Harr, bottom panels) of the Influenza NS1 genomic locus at 8 hpi. Data from the plus strand (dark blue) and the minus strand (light blue) is presented. **(C)** Ribosome footprints profile of one human gene (ISG15) at 8 hpi. **(D)** Meta gene analysis from start codon for footprints originating from viral mRNAs. Data from 2, 4 and 8 hours of IAV infected and 8 hpi-harringtonine treated cells. **(E)** Fragment length organization similarity score (FLOSS) analysis for human mRNAs and for viral reads originating from the plus and minus strands.

Fig. 3

(A) Cumulative TE distribution among well-expressed human and viral genes shows that viral genes are translated at the same efficiency as cellular genes at 2, 4 and 8 hpi. **(B)** Percent of reads that aligned to the human or viral genome from the sum of aligned reads shown for ribosome profiling (footprints) and RNA-seq (mRNA) at 2, 4, and 8 hpi. **(C)** Ribosome footprints and mRNA read densities (reads per kilobase million, RPKM) of well-expressed human transcripts across three time points during Influenza infection were calculated relative to expression of uninfected cells (mock). Shown is a heat map of log2 expression ratios after partitioning clustering. Four main clusters are marked and for each of these clusters the pathway enrichment is labeled on the left. **(D)** Validation

706 of mRNA measurements by real time qPCR for example genes. A representative analysis
707 of two independent experiments is shown
708
709 Fig. 4
710 **(A)** Western blot analysis of eIF2α and its phosphorylated form (phos- eIF2α) along IAV
711 infection. A representative blot of two independent experiments is shown.
712 **(B)** Polysomal profiling of uninfected and IAV infected cells at 4 hpi. **(C)** Real time qPCR
713 analysis of the relative levels of the indicated human mRNAs in the polysome-free
714 fractions of the gradient (F), light polysomal fractions (L), and heavy polysomal fractions
715 (H) of uninfected and IAV infected cells at 4 hpi. A representative analysis of two
716 independent experiments is shown
717
718 Fig. 5
719 **(A)** mRNA detection by Single molecule FISH (smFISH) was performed on A549 cells,
720 either mock infected or 8 hpi. DNA oligomer probes coupled with fluorescent dyes
721 (cy5/Alexa549) were targeted against viral hemagglutinin (*HA*), human *MYC* and *CHML*
722 mRNAs. Spots corresponding to single mRNA molecules were detectable. DAPI was used
723 for nuclear staining. Scale bar is 20 µm. Representative images of at least two biological
724 replicates are shown. **(B)** The numbers of mRNA molecules per cell from at least 45 cells
725 were quantified along Influenza infection (mock infection, 2, 4, 8 hpi) using smFISH. The
726 values obtained from both smFISH and RNA-seq measurements were normalized to
727 mock and plotted on the same graph. **(C)** For *CHML*, *KIF18a* and *MYC* nuclear and
728 cytoplasmic mRNA molecules were quantified using smFISH. p-values are derived from a
729 Student's *t*-test, *p < 0.05. **(D-F)** Various features were compared between transcripts
730 composing the clusters presented in Fig. 3C (representing differential response to IAV
731 infection). **(D)** mRNA half-lives measurements in A549 cells (33) **(E)** Transcripts length
732 distribution. **(F)** Transcripts GC content distribution.
733
734 Fig. 6

735 **(A)** Western blot analysis of components of the respiration complex UQCRC2, SDHB,
736 COXII, and control genes PKN2 and ACTIN along IAV infection. A representative blot of
737 three independent experiments is shown. **(B)** FACS analysis of TMRM staining for active
738 mitochondria in A549 cells, either mock infected, untreated, infected for 12 and (left
739 panel) or 24 hours (right panel). A representative analysis of two independent
740 experiments is shown. **(C and D)** A549 cells infected with IAV were treated with either
741 CCCP (untreated control, 1 µM and 2.5 µM) or Valinomycin (untreated control, 10 µM
742 and 20 µM). Supernatants were collected at 24 and 48 hpi. Viral copy numbers were
743 estimated by qPCR **(C)** and viral titers were measured by plaque assay **ia**.
744 Representative results of two independent experiments are shown.
745
746 Figure 2-figure supplement 1
747 Metagene analysis of ribosome profiling data originating from IAV minus strand.
748 Average ribosome read density profiles from IAV minus strand, aligned to the highest
749 peak found in each viral minus strand segment. Data from cycloheximide (CHX) or
750 harringtonine (Harr) pre-treatment from 8 hpi samples.
751
752 Figure 2- figure supplement 2
753 Percentage of footprints reads that aligned to IAV plus or minus strands from the sum of
754 aligned viral reads at 2, 4, and 8 hpi.
755
756 Figure 3- figure supplement 1
757 Lysates from A549 cells infected withIAV and metabolically labeled for 30-min periods
758 ending at the times shown were analyzed by SDS-PAGE and autoradiography.
759
760 Figure 5- figure supplement 1
761 Poly-A tail length of host transcripts as was previously measured from HeLa and NIH3T3
762 cells (34) were compared between transcripts composing the clusters presented in Fig.
763 3C.

Figure 5- figure supplement 2

Transcript's GC content (left) and length distribution (right) were calculated for genes encoding ribosomal proteins and respiration components, for genes in cluster 3 after omitting these functional categories (cluster 3*) and for clusters 1 and 4 presented in Fig. 3C (representing differential response to IAV infection).

Figure 6- figure supplement 1

FACS analysis of propidium iodide (PI) staining of A549 cells infected with IAV for 48 hours and treated with either CCCP (untreated, 10 μM or 20 μM) or Valinomycin (untreated, 1 μM, 2.5 μM).

Supplementary Table 1

This table presents the fold change in RPKM of human genes RNA levels (mRNA) and translation (footprints) compare to the mock sample. The numbers are an average of two independent biological repeats.

Supplementary Table 2

This table lists the concentrations of total RNA (ng/ul) extracted along IAV infection in two independent biological repeats.

Supplementary Table 3

This table provides the statistical significance value (p-value) of translationally regulated genes (Pval<0.01). Positive values represent upregulation and negative values represent downregulation at the indicated time post infection.

Materials and Methods

Cells and viruses

The cells used in this study were the human lung adenocarcinoma epithelial cell line A549. The human influenza viruses A/Puerto Rico/8/34 H1N1 used in this study were generated as previously described (Achdout H, Arnon TI, Markel G, et al. Enhanced recognition of human NK receptors after influenza virus infection. J Immunol 2003; 171:915–23). Cells were grown on 10cm plates and were infected at a multiplicity of infection (MOI) of 5. Efficiency of infection was determined by immunofluorescence with Influenza A Antibody FITC Reagent (LIGHT DIAGNOSTIC) followed by DAPI dye for nuclear staining, and confirmed that >95% of cells were infected.

Viral genomic RNA was quantified by extracting RNA from supernatant by using the NucliSENS easyMAG (BioMerieux, France). Detection of influenza A virus infection was performed by real-time reverse transcription-PCR (rRT-PCR),using TaqMan Chemistry on the ABI 7500 instrument as previously described (48).

Ribosome profiling and RNA-Seq samples preparation

Cycloheximide treatments was carried out as previously described (44). Cells were lysed in lysis buffer (20mM Tris 7.5, 150mM NaCl, 5mM MgCl2, 1mM dithiothreitol , 8% glycerol) supplemented with 0.5% triton, 30 U/ml Turbo DNase (Ambion) and 100µg/ml cycloheximide, ribosome protected fragments were then generated as previously described (44). Total RNA was isolated from infected cells using Tri-Reagent (Sigma). Polyadenylated RNA was purified from total RNA sample using Oligotex mRNA mini kit (Qiagen). The resulting mRNA was modestly fragmented by partial hydrolysis in bicarbonate buffer so that the average size of fragments would be ~80bp. The fragmented mRNA was separated by denaturating PAGE and fragments 50-80 nt were selected and sequencing libraries were made as previously described (44).

Sequence alignments, normalization and clustering

Prior to alignment, linker and polyA sequences were removed from the 3' ends of reads. Bowtie v0.12.7 (5) (allowing up to 2 mismatches) was used to perform the alignments. First, reads that aligned to human rRNA sequences were discarded. All remaining reads were aligned to the concatenated viral (EF467817 - EF467824) and human (hg19) genomes. Finally, still-unaligned reads were aligned to the human known canonical transcriptome that includes splice junctions. Reads with unique alignments were used to compute the total number of reads at each position. Footprints and mRNA densities were calculated in units of reads per kilobase per million (RPKM) in order to normalize for gene length and total reads per sequencing run.

The expression patterns were examined for genes that had more than 150 uniquely aligned reads of mRNA and footprints. Partitioning clustering was performed using Partek Genomic suits across mRNA and footprints data. GO enrichment analysis was done using DAVID database (49). The Babel computational framework was used to quantitatively evaluate if there are genes that are differently translated along IAV infection (25).

^{35}S-labelling of nascent proteins

Infected A549 cells (mock, 2 hpi, 4 hpi, 8 hpi) were incubated in methionine depleted DMEM for 30 minutes. Subsequently, 50 µCi/mL [^{35}S]-methionine was added and incubated for 30 minutes. Cells were harvested using RIPA buffer. Lysates were run on a polyacrylamide (PAA) gradient gel (4-12%). The PAA gel was fixed overnight in a fixation solution (3% glycerol, 20% methanol, 7% acetic acid). Typhoon FLA 7000 from GE Healthcare Life Sciences was used for acquisition.

Polysome profiling

Four hours post infection A549 cells were treated with 100 µg/ml Cycloheximide for 1 minute and then washed twice with cold PBS containing 100 µg/ml Cycloheximide. The cells were collected and lyzed with 400 µl lysis buffer (20mM Tris 7.5, 150mM NaCl, 5mM MgCl2, 1mM dithiothereitol) supplemented with 0.5% triton, 30U/ml Turbo DNase

(Ambion) and 100 µg/ml Cycloheximide. The lyzed samples were centrifuged at 12,000g at 4°C for 10 minutes. The cleared lysates were loaded onto 10-50% sucrose gradient and centrifuged at 35,000 RPM in a SW41 rotor for 3 hours at 4°C. Gradients were fractionated and the optical density at 254 nm was continuously recorded using Biocomp gradient station.

Real-time PCR

RNA was isolated using Tri-Reagent (Sigma) and Direc-Zol RNA mini-prep kits (Zymo Research). cDNA was prepared from 1ug RNA except for polysomes profiling experiments in which 255ng RNA was used with High-Capacity cDNA Reverse Transcription Kit (ABI). Real time PCR was performed using the SYBR Green PCR master-mix (ABI) on a real-time PCR system StepOnePlus™ (life technologies) with the following primers:

Gene	Forward primer	Reverse primer
TBX3	CGAAGAAGAGGTGGAGGACG	AAACATTCGCCTTCCCGACT
UCP2	AGCCCACGGATGTGGTAAAG	CTCTCGGGCAATGGTCTTGT
RALGDS	GGTAGATTGCCAGAGCTCCA	CCTTGTTGCCTCCGTGGT
SOX4	GCACTAGGACGTCTGCCTTT	ACACGGCATATTGCACAGGA
SF3B5	GCGACTCGTACTGCTCCTAC	CTCGCGCTTTGCTCTCATTC
LAMP2	CCGGCTTCTGGAGTAAGGTA	CAGGTGTACAAAGCAGCCAT
IFI6	TACACTGCAGCCTCCAACTC	AGTTCTGGATTCTGGGCATC
NR4A1	GTCCTGGGTCCAGTAGGAAA	GAGGAGTGGGACTGACCAAT

smFISH

Probe library constructions, hybridization procedures, and imaging conditions were described previously (30). In short, probe libraries consisted of 48 probes of length 20 bases, were coupled to cy5 (for *MYC*, and KIF18A) or alexa594 (for *CDKN1B*, *HA* and

CHML). Hybridizations were performed overnight in 30°C. DAPI dye for nuclear staining was added during the washes. Images were taken with a Nikon Ti-E inverted fluorescence microscope equipped with a ×100 oilimmersion objective and a Photometrics Pixis 1024 CCD camera using MetaMorph software (Molecular Devices, Downington, PA). Quantification was done on stacks of 10-15 optical sections, with Z spacing of 0.2 µm.

Fragment Length Organization Similarity Score (FLOSS)

The FLOSS score was computed as previously described (19). Briefly, a histogram of read lengths for all footprints that aligned to a specific transcript or reading frame was calculated and compared to a reference histogram produced by summing individual raw counts (without normalization) for annotated nuclear transcripts.

Examination of various features of cellular transcripts

The transcripts composing the clusters presented in figure 3C were analyzed. For each cluster, we examined recently published data of RNA half-life in A549 cells (33). In addition, we examined the mean poly(A) tail length from measurements that were performed in HeLa and NIH3T3 cells (34). Transcripts length and GC content was calculated excluding introns. For each feature, pairs of clusters were compared using a two-sided t-test except for RNA half-life in which the clusters were compared using the Mann-Whitney test. Presented is the largest p-value of the three comparisons.

Western blots analysis and drug treatments

Infected A549 cells and the mock control were harvested 2 hpi, 4 hpi 8 hpi, 12 hpi, 16 hpi using RIPA Buffer. Membrane was blocked for 1 h in 5% Skim milk TBST. Primary antibodies UQCRC2, SDHB, COXII (ab110413, Abcam), PKN2 (ab32395, Abcam), ACTIN (A4700, Sigma Aldrich), eIF2α (sc-11386, Santa Cruz) and phosphorylated (S52) eIF2α (447286, Invitrogen) were diluted 1:1000 in 5% BSA TBST and incubated for 1 h at RT or over night at 4°C. Secondary antibodies IRDye® 680RD goat anti-rabbit (LIC-92668071)

and IRDye® 680RD goat anti-mouse (LIC-92668070) were diluted 1:10000 in 5% Skim milk TBST and incubated for 1 h at RT. Acquisition was performed using , Odyssey® CLx from LI-COR. A549 cells were treated after 2 hpi (IAV) with CCCP (untreated, 10 µM or 20 µM) or Valinomycin (untreated, 1 µM, 2.5 µM). For Tetramethylrhodamine (TMRM) staining A549 cells were incubated with 20 nM TMRM in 1ml of DMEM for 30 min at 37°C, prior analysis in the flow cytometer. For PI (propidium iodide) staining, target cells were resuspended in 100 µL PBS and 10 µL staining solution (10 µg/mL PI in PBS) was added for 1 minute prior to acquisition in the flow cytometer.

Plaque assay

Confluent MDCK cells were incubated for 1 h at 37°C with 0.5 ml 10-fold serial dilutions of virus in 6-well plates, present in DMEM medium supplemented with 3µg/mL IX-S trypsin (sigma T-0303). The cells were then washed and overlaid with freshly prepared DMEM containing 1.5% Agarose. The plaques were visualized after incubation at 37°C for 3 days by staining with 0.3% crystal violet solution containing 20% ethanol.

Figure 1

A

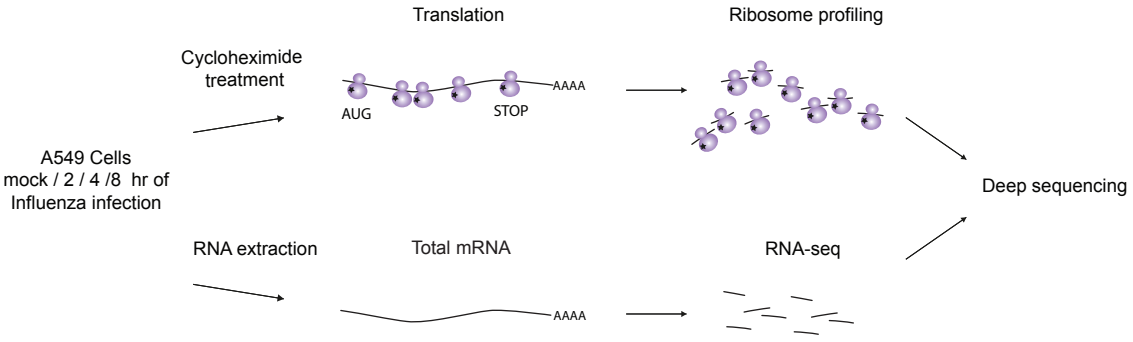
Translation
Ribosome profiling
Cycloheximide
treatment
AUG
STOP
AAAA
A549 Cells
mock / 2 / 4 /8 hr of
Influenza infection
Deep sequencing
RNA extraction
Total mRNA
RNA-seq
AAAA

B

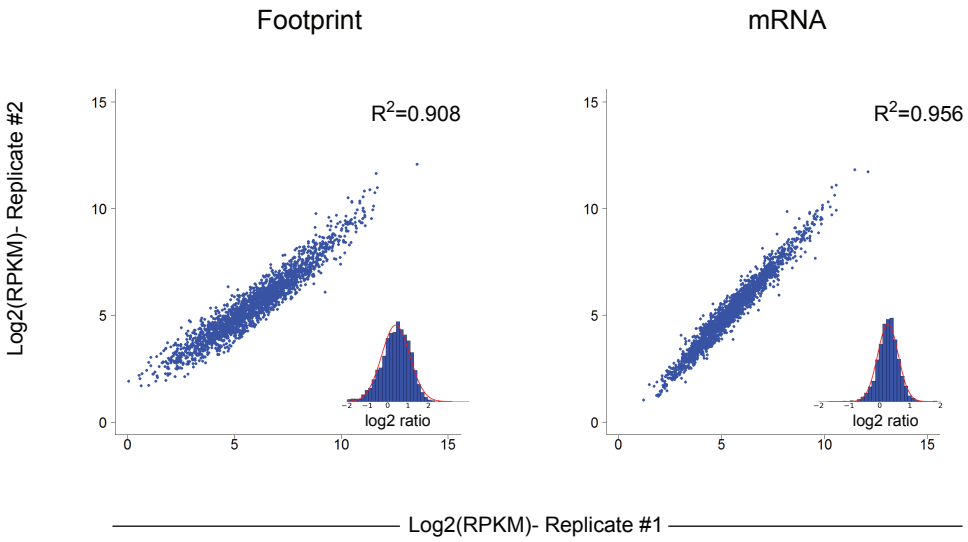
Footprint
mRNA
Log2(RPKM)- Replicate #2
R2=0.908
R2=0.956
log2 ratio
log2 ratio
Log2(RPKM)- Replicate #1

Figure 2

A

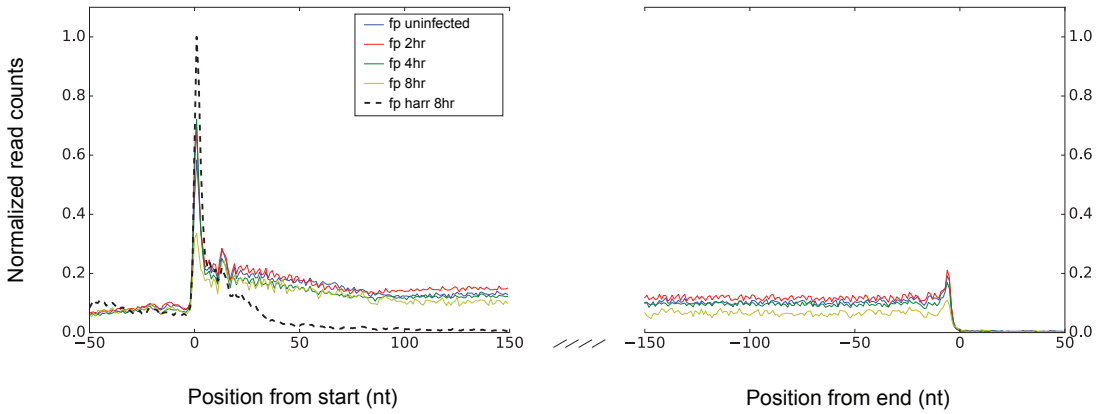

B

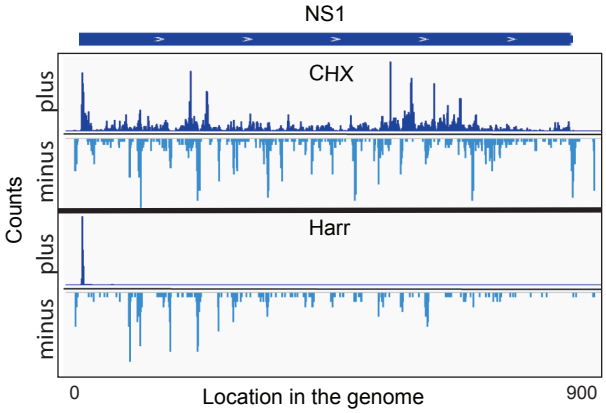

C

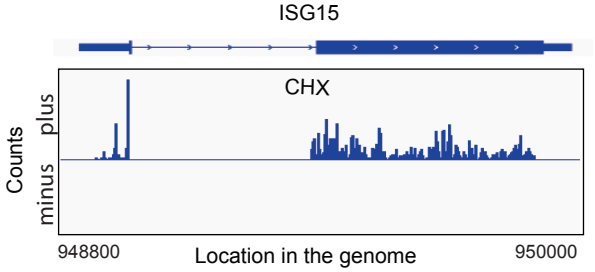

D

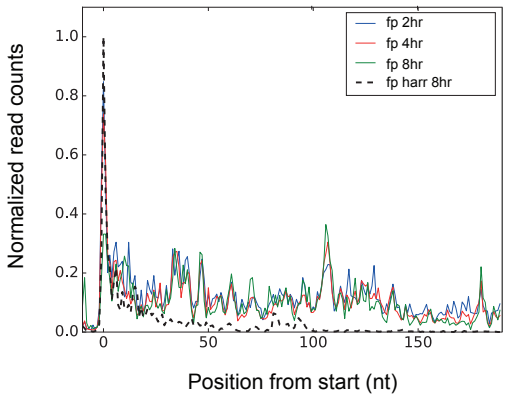

E

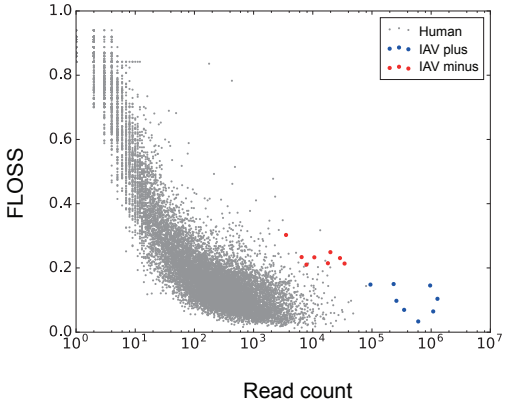

Figure 3

A

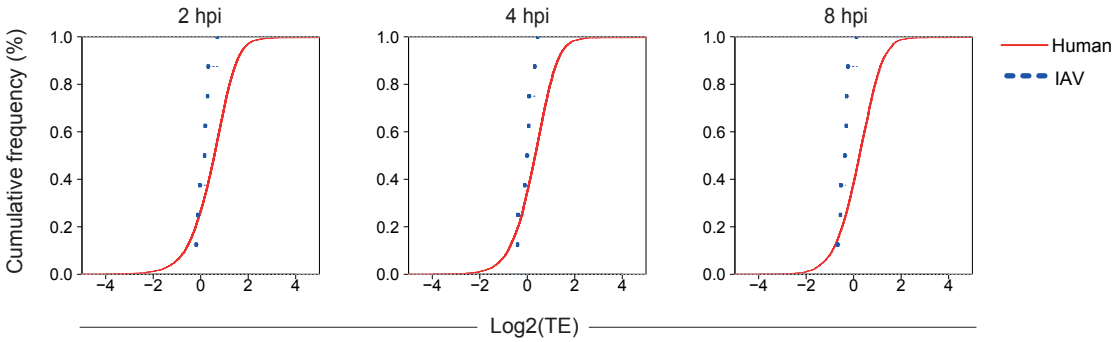

B

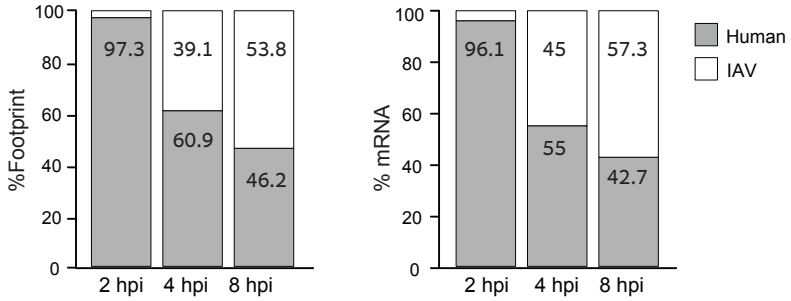

C

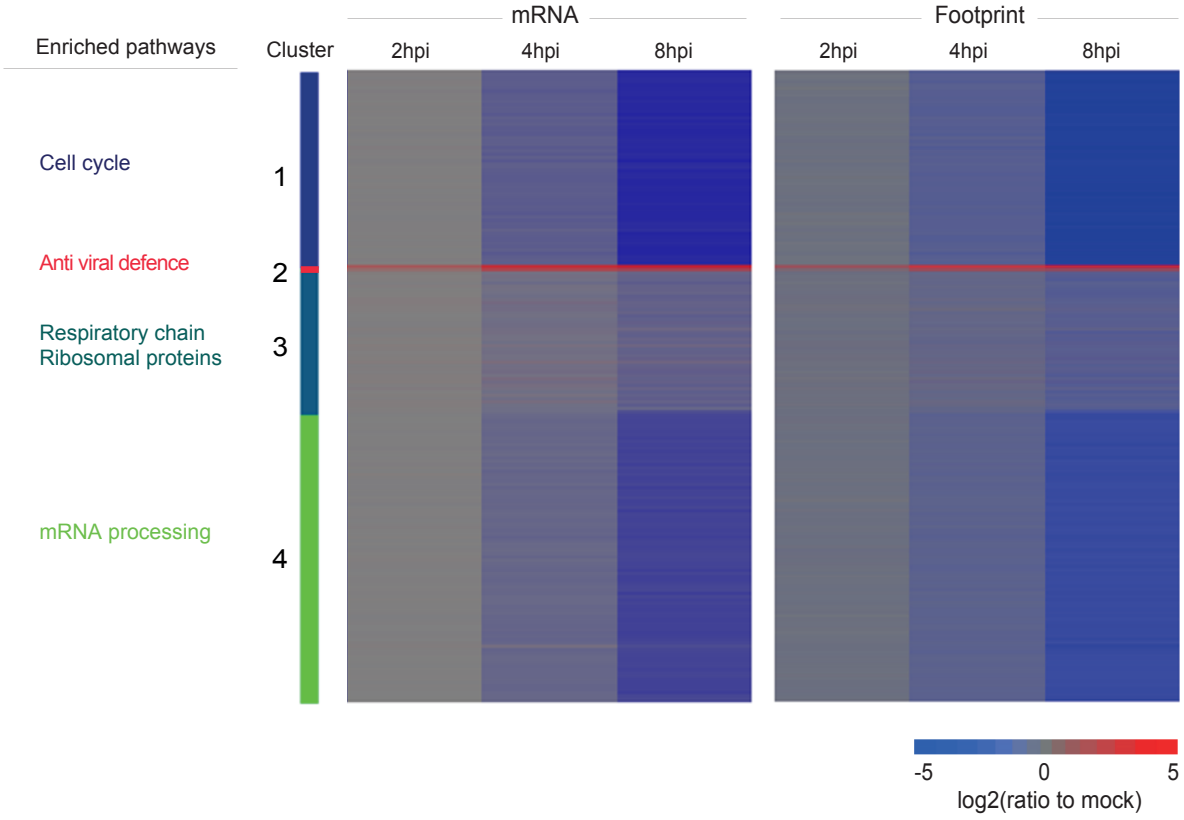

D

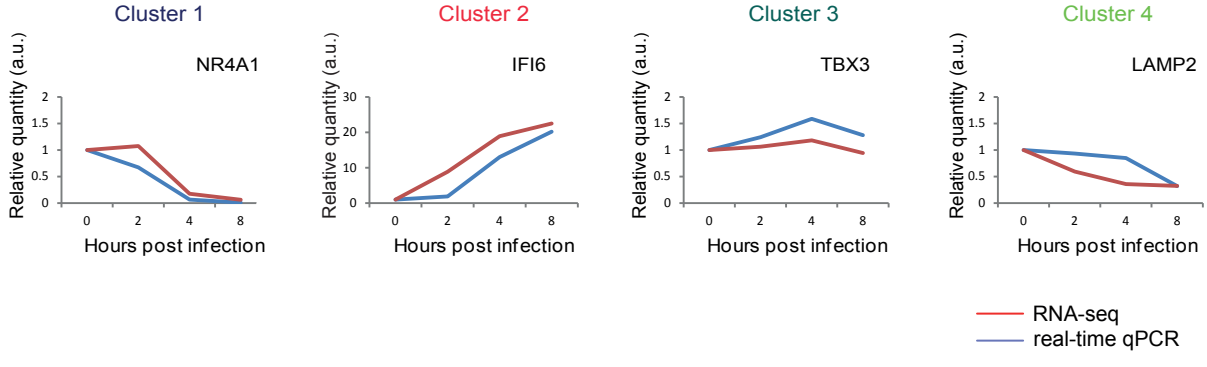

Figure 4

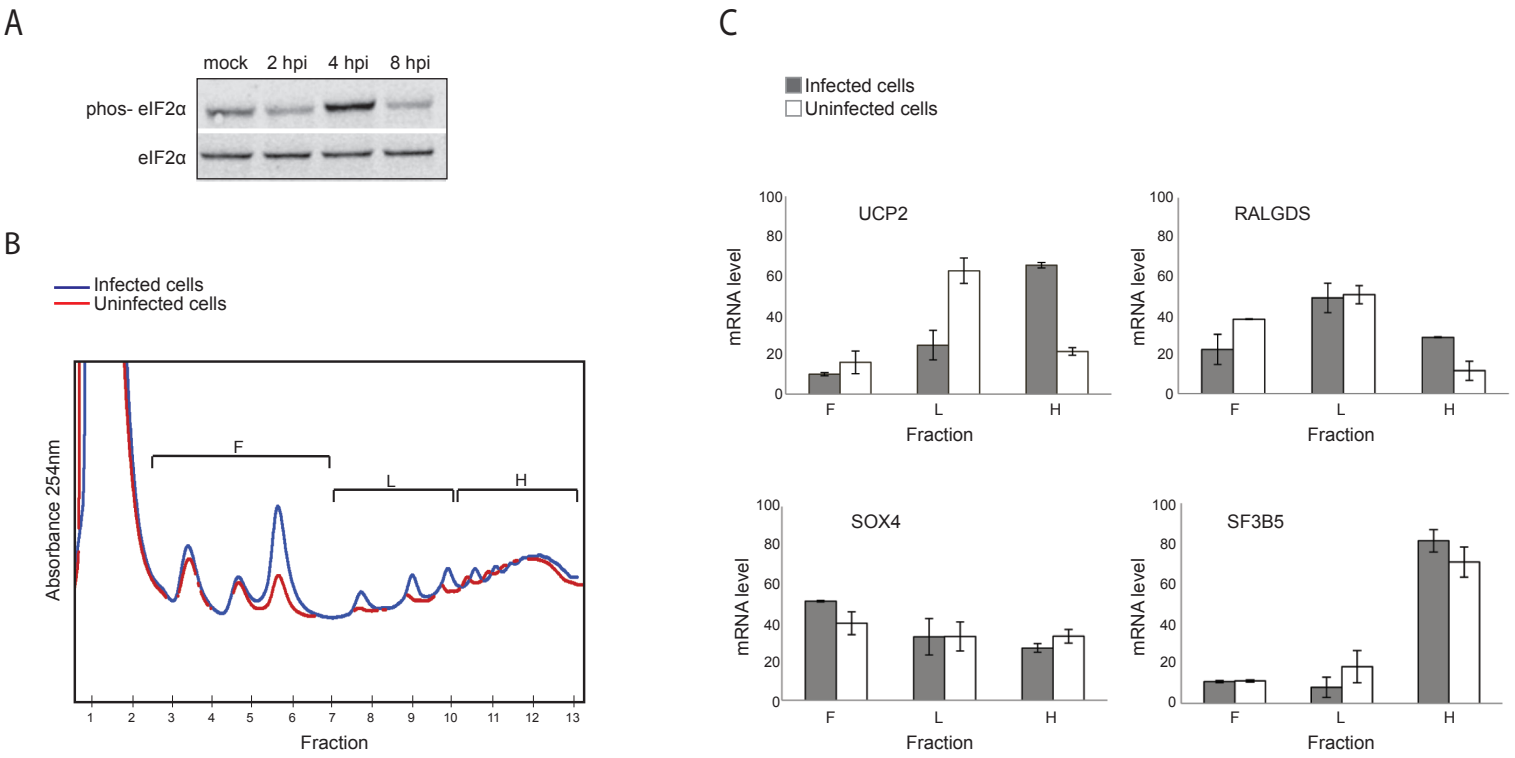
A
mock
2 hpi
4 hpi
8 hpi
phos- eIF2α
eIF2α
B
Infected cells
Uninfected cells
Absorbance 254nm
F
L
H
1
2
3
4
5
6
7
8
9
10
11
12
13
Fraction
C
Infected cells
Uninfected cells
UCP2
RALGDS
SOX4
SF3B5
mRNA level
100
80
60
40
20
0
F
L
H
Fraction

Figure 5

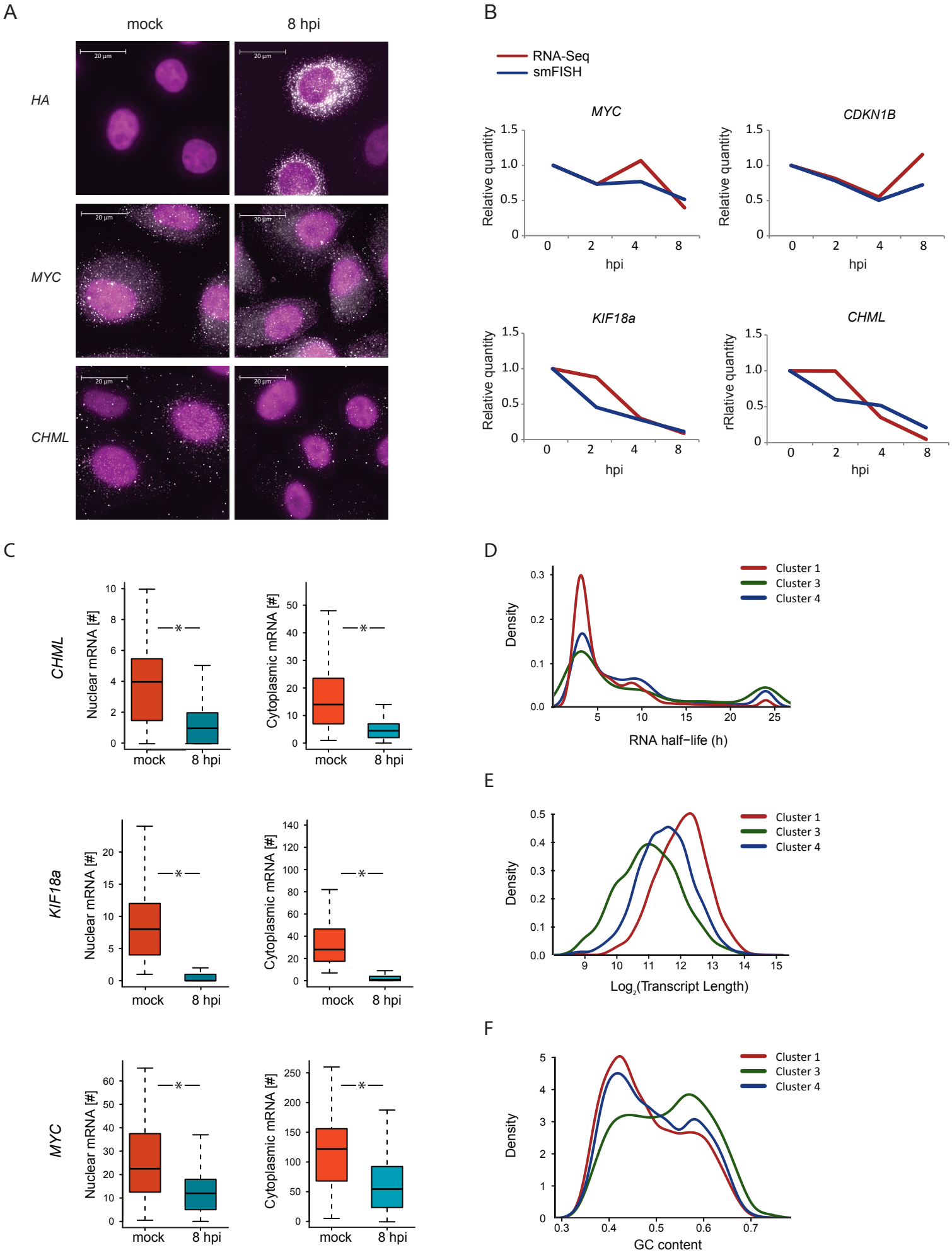
A
mock
8 hpi
HA
MYC
CHML
20 µm
B
RNA-Seq
smFISH
MYC
CDKN1B
KIF18a
CHML
Relative quantity
rRlative quantity
hpi
C
CHML
KIF18a
MYC
Nuclear mRNA [#]
Cytoplasmic mRNA [#]
mock
8 hpi
D
Cluster 1
Cluster 3
Cluster 4
Density
RNA half−life (h)
E
Log2(Transcript Length)
F
GC content

Figure 6

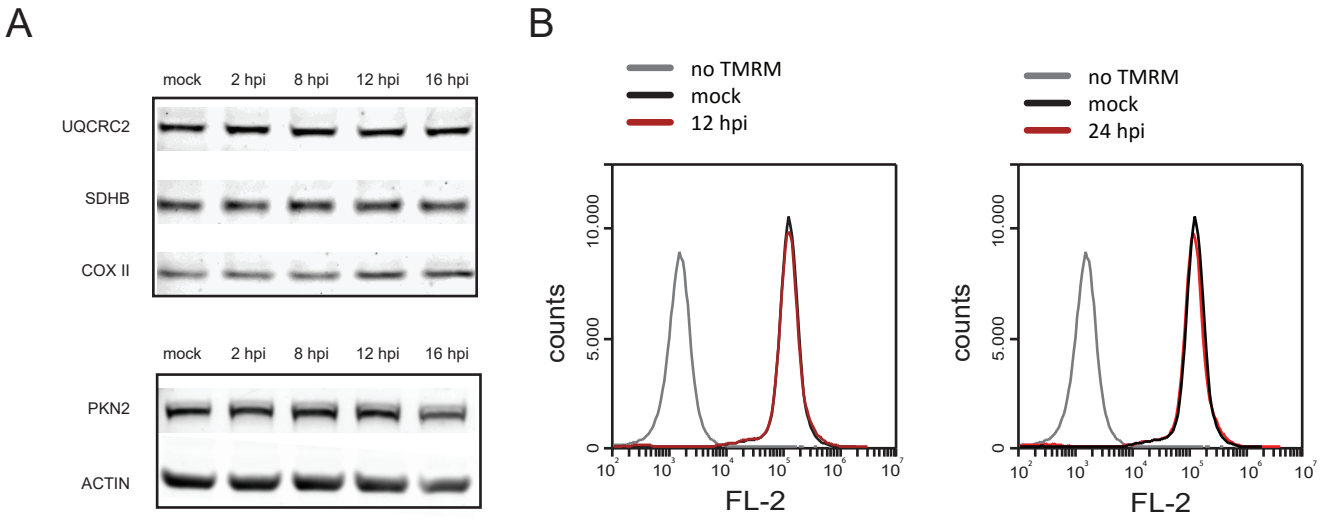
A
mock
2 hpi
8 hpi
12 hpi
16 hpi
UQCRC2
SDHB
COX II
PKN2
ACTIN
B
no TMRM
mock
12 hpi
24 hpi
counts
FL-2

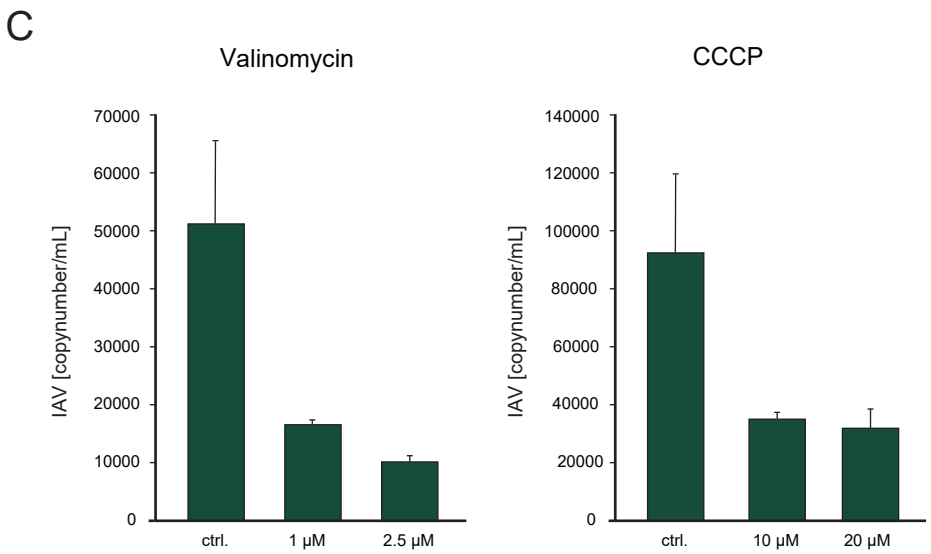
C
Valinomycin
CCCP
IAV [copynumber/mL]
ctrl.
1 µM
2.5 µM
10 µM
20 µM

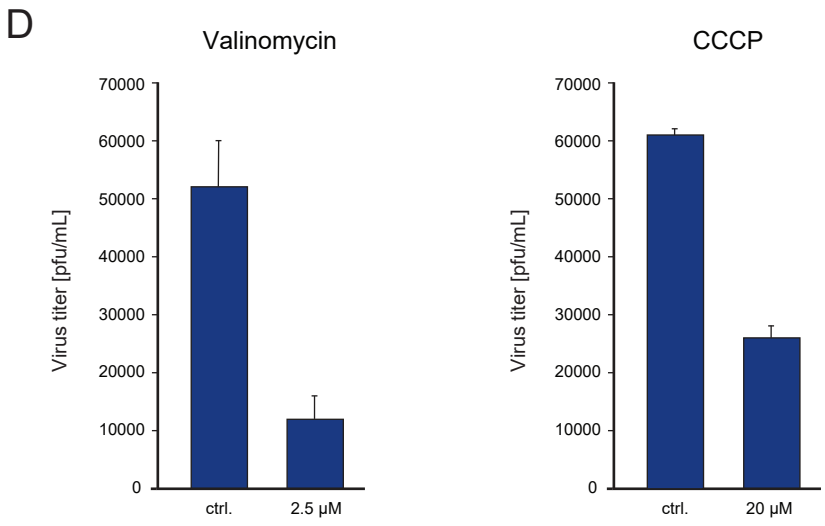
D
Valinomycin
CCCP
Virus titer [pfu/mL]
ctrl.
2.5 µM
20 µM